IEEE Access
Multidisciplinary ⋮ Rapid Review ⋮ Open Access Journal

Received May 3, 2021, accepted May 26, 2021, date of publication May 28, 2021, date of current version June 8, 2021.

Digital Object Identifier 10.1109/ACCESS.2021.3084857

Analysis of Intersymbol Interference Characterized by the Large Array Antennas Adopted in a 60-GHz-Band Gigabit Compact-Range Wireless Access System

MIAO ZHANG[1,2], (Senior Member, IEEE), MASAHIRO WAKASA[2], KOJI TOYOSAKI[2], KIYOMICHI ARAKI[2], (Life Member, IEEE), JIRO HIROKAWA[1,2], (Fellow, IEEE), AND MAKOTO ANDO[2], (Life Fellow, IEEE)

[1]Institute of Electromagnetics and Acoustics, Xiamen University, Xiamen 361005, China
[2]Department of Electrical and Electronic Engineering, Tokyo Institute of Technology, Tokyo 152-8552, Japan

Corresponding author: Miao Zhang (miao@xmu.edu.cn)

This work was supported in part by the National Natural Science Foundation of China under Grant 61971364, and in part by "the Research and Development for Expansion of Radio Wave Resources" under the contract of the Ministry of Internal Affairs and Communications, Japan.

ABSTRACT A compact-range wireless access system in the 60-GHz band has been proposed for multi-Gb/s data transfer. A prototype Gigabit Access Transponder Equipment (GATE) was built to evaluate the system performance in terms of received signal strength, signal-to-noise ratio (SNR), and bit error rate (BER). The proposed system operates in the near-field regions of large array antennas adopted in the transmitter (Tx). The time delays due to the signals transmitted from different array elements to the receiver (Rx), or/and those due to the multiple reflections between Tx and Rx antennas become comparable with the symbol lengths in our gigabit wireless access system. In that sense, this system would be susceptible to intersymbol interference (ISI). In this study, the concept of ISI is introduced in the antenna field for the first time. An equivalent baseband communication system is newly proposed to evaluate the wireless channel, including Tx and Rx antennas. The analysis procedures and equations are provided for the calculation of ISI. The ISIs due to three potential contributions are analyzed in detail. It is verified that our proposed ISI analysis has succeeded in relating the antenna characteristic to the system performance observed in the baseband.

INDEX TERMS Intersymbol interference, compact-range communication, large array antenna, near-field region, symbol rate, delay spread, multiple reflections, signal-to-noise ratio, bit error rate.

I. INTRODUCTION

Gigabit wireless communications attract increasing attention from industry in recent years. The global activities in the research and development of high-speed and high-capacity wireless communication systems are intensified by the emerging fifth-generation (5G) mobile network [1], [2]. The aggressive usages of extremely-high frequency resources represented by the millimeter-waves [3], [4], including the Q-band, V-band, E-band, and other higher frequency bands, secure a wide bandwidth of multi-GHz frequency. As a trend, both the radio frequency and the symbol rate are accreting rapidly. Meanwhile, those emerging gigabit wireless communication systems employing the millimeter-waves could significantly suffer even from short delays, which become comparable with the short symbol lengths. This phenomenon, which has never been observed in present wireless systems, is profoundly unique.

A novel compact-range wireless access system in the 60-GHz band was proposed to realize multi-Gb/s data transfer [5]. A GATE (Gigabit Access Transponder Equipment), together with mobile terminals, enables the burst-type access to a cloud service. As illustrated in Fig. 1, the 60-GHz-band GATE is to be equipped as the fixed access point in public areas such as in corridors and escalators located in stations and department stores. When a user holding a mobile terminal passes through a GATE, the gigabit access is available in its coverage area, clearly defined by a large array antenna. In addition, the distance-independent line of sight (LOS) propagation and multipath-free radio

The associate editor coordinating the review of this manuscript and approving it for publication was Lu Guo.

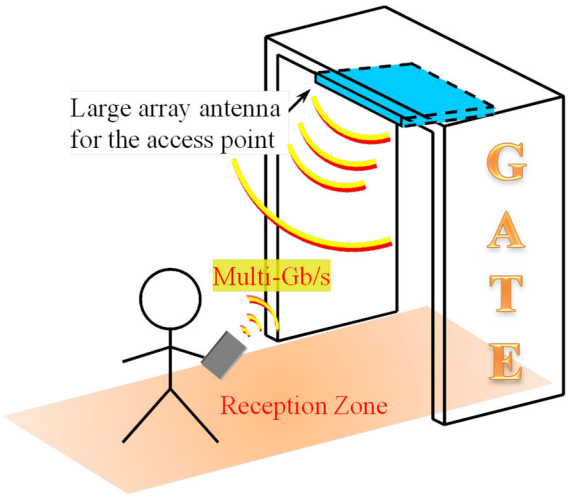

FIGURE 1. 60-GHz-band GATE for compact-range wireless access system.

environment enables the single-carrier signal transmission with disregard of fading and sophisticated equalization techniques. The conventional mobile communication and the fixed wireless access (FWA) system generally operate in their far-field regions. In contrast with them, the compact-range wireless access system suggests a new wireless communication category.

Moreover, this compact-range wireless access system operates in the near-field regions of large array antennas. The communication distance becomes comparable with the large aperture sizes of Tx (Transmitter) antennas. The signals transmitted from different elements, which are spatially distributed in a large Tx array, may contribute to considerable time delays and eventually cause critical intersymbol interference (ISI) [6] in the Rx (Receiver). Furthermore, the multiple reflections occurring between Tx and Rx antennas or/and occurring within the Tx antenna itself may also contribute to a significant degradation in ISI. Generally, flat group delays over the operating frequency range are required when designing ultra-wideband (UWB) antennas [7], [8]. However, there were no practical ways to relate the wireless channel, including both Tx and Rx antennas, directly with the overall system quality evaluated in the baseband (BB). Our proposal can provide a straightforward solution to this problem in a quantitative way.

In this paper, we analytically investigate the ISI occurring in the wireless channel of a compact-range wireless access system. An equivalent baseband communication system is newly proposed to evaluate the wireless channel, including both Tx and Rx antennas. The analysis procedures and equations are provided for the calculation of ISI = 1/SIR (Signal-to-Interference Ratio). When the noise is neglected, this SIR can be directly approximated as an overall SINR (Signal-to-Interference-plus-Noise Ratio) observed in BB. The bit-error-rate (BER) is then ready to be read from the theoretical curve relating BER to SINR for a specific modulation. We evaluate the ISI first as a function of the Tx-Rx distance in a wireless channel, whose transfer function is analytically available. Its dependence on the aperture size of a Tx antenna is investigated as well. On the other hand, the transfer function can also be obtained by directly connecting the prototype 16 × 16 and 64 × 64-element arrays with a vector network analyzer (VNA). The ISIs due to the multiple reflections between Tx and Rx antennas or/and within the Tx antenna itself are further evaluated.

The newly proposed ISI analysis will succeed in relating the antenna characteristic to the system performance represented by SINR and BER observed in BB. Furthermore, it can be applied to other wideband systems such as the UWB system [7], [9], millimeter-wave wireless links in the E-band [10]–[14], D-band [15], [16], *et al.* In the future, this ISI analysis will help us to draw up new guidelines when designing large array antennas to be adopted in the high-speed near-field communication systems.

II. SYSTEM EVALUATION OF A PROTOTYPE GATE

A prototype GATE, including a BB module [17] and an RF (Radio Frequency) front-end [18], was constructed for demonstration. This system utilized a 2.16-GHz frequency bandwidth ranging from 59.40 to 61.56 GHz (Channel 2). The channel-bit rate was as high as 3.456 Gb/s for the $\pi/2$-shift quadrature-phase-shift keying (QPSK) modulation. By adopting a low-density parity-check (LDPC) code with a 14/15 rate [19], we acquired the maximum data rate of 3.1 Gb/s in an efficient way.

The circularly-polarized waveguide slot arrays with various aperture sizes were designed and fabricated in the V-band [20]. The small antennas represented by the 2 × 2 and 4 × 4-element arrays and the large antennas represented by the 32 × 32 and 64 × 64-element arrays were used as Tx antennas. Here, the element spacing for all antennas was 4.2 mm in common [5]. Meanwhile, an open-ended waveguide probe with linear polarization (LP) was used as the Rx antenna in common. The accessibility and user-friendliness can be enhanced by adopting the circular polarization (CP) in the Tx antenna, since the user is unnecessary to adjust the orientation of a mobile terminal. Hence, it is convenient to adopt CP in Tx, and simultaneously adopt LP in Rx for simplicity. Even though the array antenna in Tx had numerous radiating elements, only one RF input was connected to the Tx antenna. In an initial development phase, the prototype GATE was a SISO (Single-Input Single-Output) system rather than a MIMO (Multiple-Input Multiple-Output) one.

The position of Tx was fixed, and Rx moved longitudinally along the z-direction. The system SINRs and BERs without LDPC for various Tx antennas were measured as summarized in Fig. 2. For the 2 × 2 and 4 × 4-element arrays, the BERs degrade fast with increment in the propagation distance due to the decrement in the Rx-RF signal strength as well as the SNR. A communication zone up to 11 m, characterized by the SNR higher than 11 dB and the BER lower than 10^{-4} without LDPC, was realized by adopting the 32 × 32 and 64 × 64-element arrays in Tx. It was worth noting in Fig. 2, the measured BERs for the 32 × 32-element array were

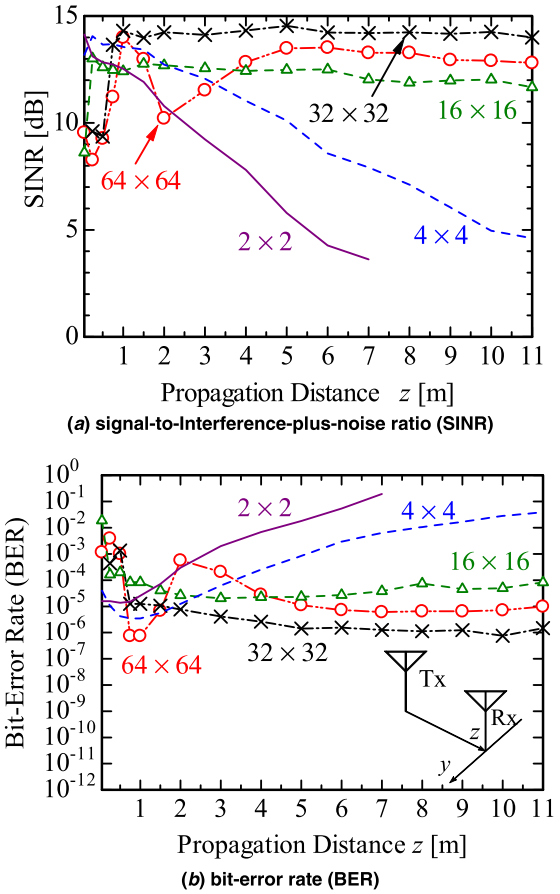

FIGURE 2. Measured SINRs and BERs without LDPC as a function of propagation distance z for various antennas.

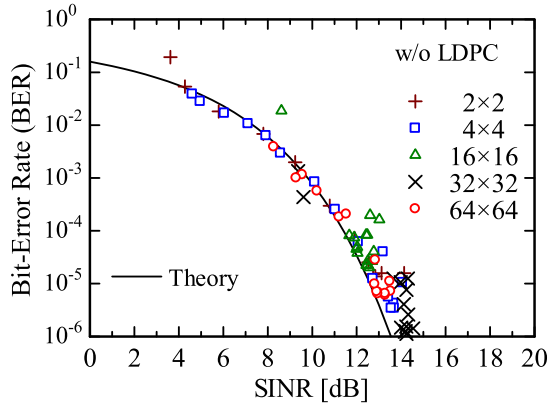

FIGURE 3. Measured BERs without LDPC as a function of SINRs.

better than those for the 64 × 64-element one. As detailed in [5], the 32 × 32-element array had advantages over the 64 × 64-element one in terms of both aperture uniformity and impedance matching. Nonetheless, a quantitative evaluation relating the defective antenna performance to the system SINR remained an issue for us.

Additionally, the relations between BERs and SNRs were investigated as well. The measured BERs without LDPC for all five Tx antennas were plotted as a function of the measured SNRs in Fig. 3, where their theoretical curve for the modulation of QPSK was also reproduced by assuming an AWGN (Additive White Gaussian Noise) channel [21]. Good agreement was observed in Fig. 3. It was verified that the fading effect was almost negligible, and a LOS propagation environment was reasonably realized in our present compact-range wireless access system, especially when the Rx was separated from the Tx at a distance of more than 1 m.

However, as shown in Fig. 2, the BERs without LDPC for the 32 × 32 and 64 × 64-element arrays degrade drastically when the propagation distance is less than 1 m. This unique phenomenon deserves careful investigations.

III. INTRODUCTION OF INTERSYMBOL INTERFERENCE

For better comprehension, the novelties and system features of the 60-GHz-band compact-range gigabit wireless access system are reexamined and summarized as follows:

– First, this compact-range communication makes itself distinct from both the conventional mobile communication and the fixed wireless access and belongs to a new wireless communication category. That is, a LOS propagation environment is indispensable here in contrast to the mobile communication; meanwhile, further mobility is available here compared to the fixed wireless access.

– Second, the symbol rate in the prototype GATE is as high as 1.728 GS/s [17]. That is, the symbol length is as short as 0.579 ns. In that sense, the system would be susceptible even to a short delay time at a nanosecond level. For example, the propagation path-difference as short as 17.35 cm corresponds to the delay equal to one symbol length of 0.579 ns.

– Third, this proposed indoor system is a simple SISO system instead of a massive-MIMO one, even though a large array antenna with as many as 32 × 32 or 64 × 64 elements is installed in the access point.

– Fourth, since the proposed system adopting a large array antenna in Tx is operating in its close near-field region, the signals transmitted from spatially different array elements have unequal arrival times at the user terminal. The delay and delay spread become more critical when the Rx approaches the Tx, as observed in Fig. 2.

Since the delay spread is also comparable with the above-mentioned symbol length, the same symbols transmitted from different array elements can severely interfere with each other within the wireless channel. This unique phenomenon has inspired us to introduce ISIs in investigating our proposed system. Furthermore, when evaluating a wireless channel including Tx and Rx antennas, successful acquisition of the overall transfer function becomes a critical issue. It can efficiently characterize not only the multiple reflections between Tx and Rx antennas but also group delays as well as multiple reflections within the antenna feeding circuits.

As far as we know, the ISI has never been considered before in the antenna field. From now on, when designing antennas for a gigabit compact-range wireless access system, the antenna engineers should take into account ISI in addition to the conventional far-field indices such as antenna gain, directivity, *et al.* The radiation patterns in terms of positions (x, y, z) rather than directions (θ, ϕ) should be examined and

optimized especially in the near-field applications. Of course, the evaluations of impedance matching, radar cross section (RCS), etc. remain crucial as before. However, it is only known for us in a qualitative way that the return loss and fluctuations in antenna gains within the operating frequency range can degrade the system performance. Our ISI analysis to be proposed in this paper can quantitatively relate the antenna performance evaluated in the wireless channel to the system performance evaluated in BB. Hence, two approaches developed for designing the far-field and near-field antennas can be complementary to each other, and can also help each other enhance both antenna performance and system performance.

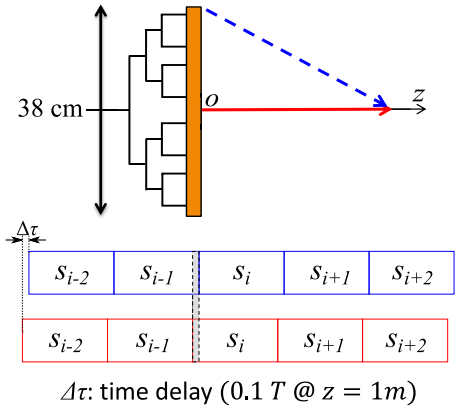

FIGURE 4. Calculation of time delay between the signals sending from the center and edge of a corporate-fed linear array.

For a better illustration of ISI's mechanism, a simple antenna model is examined here. As shown in Fig. 4, a corporate-fed linear array with a maximum dimension of 38 cm is adopted as the Tx antenna. Ideally, there is no delay occurring within the antenna feeding circuit. s_i is the i-th symbol simultaneously send from the spatially different elements of the Tx antenna. We pay close attention to two signals sent from the center and edge elements. They are denoted by the solid and dashed arrows, as illustrated in Fig. 4. When the Rx is positioned at a distance of 1 m along the central axis, the delay between those two signals becomes one-tenth of the symbol length. The overlapped region, marked in gray color shown in Fig. 4, corresponds to the interference of symbols s_i in the time domain.

Three potential contributions to critical ISIs are briefly summarized as follows.

–First, the significant delay spread due to the size of a large array antenna in Tx may be dominant, especially when its aperture size is comparable to the Tx-Rx distance.

–Second, the multiple reflections between Tx and Rx antennas may significantly degrade the ISI as well. The RCSs, including both the structural mode and the antenna mode scattering [22], [23], mainly determine the loop gain between those two antennas. Especially when the antennas are positioned in their near-field regions, the near-field RCSs should be adopted, and the Rx-RF signal strength not following the Friis Transmission Equation should be kept in mind. By the way, the abovementioned two contributions, i.e., delay spreads due to large antenna apertures and multiple reflections between Tx and Rx antennas, have opposite dependence on the Tx-Rx distance.

–Third, the matching condition and the group delay within the feeding circuit may further degrade the ISI significantly. It is worth noting that this contribution is independent of the Tx-Rx distance, and in part affects the "noise floor" in SINR.

In this paper, we focus on the ISI analysis. Meanwhile, other essential approaches to analyzing the propagation environment are under development. For example, a signal flow graph model [24] has been proposed initially to obtain the distance-dependent transfer function, where the RCS is a key parameter to present the overall performance of an Rx antenna operating in the near-field region of a Tx antenna. On the other hand, the high-frequency approximation methods, including GTD (Geometrical Theory of Diffraction), UTD (Uniform Theory of Diffraction), and MER (Modified Edge Representation), have been applied to evaluate the shadowing effect efficiently [25].

IV. ANALYSIS OF INTERSYMBOL INTERFERENCE

A. ANALYSIS MODEL AND CALCULATION OF ISI

In this study, the main issue is to investigate the wireless channel, including Tx and Rx antennas. As illustrated in Fig. 5, an equivalent BB communication system [26] is proposed by neglecting the frequency conversion between BB and RF circuits. For simplicity, neither the white Gaussian noise within the wireless channel nor the other noise figures due to other circuit components in our prototype GATE are considered here. In that sense, the SINR is simplified as SIR. To some extent, the ISI analysis here is more like a qualitative evaluation rather than a rigorously quantitative one. The analysis procedure and calculation of ISI are detailed as follows.

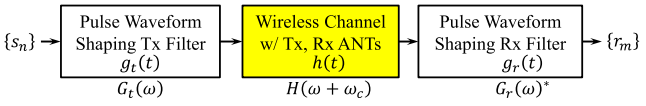

FIGURE 5. Proposed equivalent baseband (BB) communication system.

As illustrated in Fig. 5, the transfer function of a wireless channel is represented by $H(\omega+\omega_c)$. The frequency spectra of the pulse waveform shaping filters in Tx and Rx are $G_t(\omega)$ and $G_r(\omega)^*$, respectively. Here, ω_c is the center angular frequency of the RF carrier. Generally, when $G(\omega) = G_t(\omega) G_r(\omega)^*$ behaves in a raised cosine spectrum, the condition of a Nyquist criterion is automatically satisfied [6]. That is, the intersymbol interference is ideally zero when there is no delay occurring within the wireless channel. A roll-off factor $\alpha = 0.25$ [17] is adopted in both our prototype GATE and the abovementioned equivalent BB communication system.

$\{s_n\}$ is the transmitted binary sequence to be transmitted. Then the transmitted signal spectrum $S(\omega)$ produced by one pulse waveform shaping filter in Tx can be expressed as follows.

$$S(\omega) = \sum\nolimits_n s_n G_t(\omega) e^{-j\omega nT} \tag{1}$$

Here, the symbol length T of 0.579 ns corresponds to the symbol rate of 1.728 GS/s in our prototype GATE.

On the opposite side of the wireless channel, the received signal spectrum $R(\omega)$ is equal to $S(\omega) H(\omega + \omega_c)$. After it passes through the other pulse waveform shaping filter as the counterpart in Rx, the received binary r_m can be expressed in the following equation.

$$\begin{aligned} r_m &= \int R(\omega) G_r(\omega)^* d\omega/(2\pi) \\ &= \sum\nolimits_n s_n \int G_t(\omega) e^{-j\omega nT} H(\omega + \omega_c) e^{j\omega mT} \\ &\quad \times G_r(\omega)^* d\omega/(2\pi) \\ &= \sum\nolimits_n s_n \int G(\omega) H(\omega + \omega_c) e^{j\omega(\mathrm{m-n})T} d\omega/(2\pi) \\ &= \sum\nolimits_n s_n K_{m-n} \end{aligned} \tag{2}$$

$$K_{m-n} \int G(\omega) H(\omega + \omega_c) e^{j\omega(\mathrm{m-n})T} d\omega/(2\pi) \tag{3}$$

Here, K_{m-n} is defined as the interference sequence. Finally, the ISI defined as the ratio of interference to signal can be formulated as follows:

$$\begin{aligned} \mathrm{ISI} &= \frac{\text{Interference}}{\text{Signal}} = \frac{\left|\sum_n s_n K_{m-n}\right|^2 - \max_n |s_n K_{m-n}|^2}{\max_n |s_n K_{m-n}|^2} \\ &= 1/\mathrm{SIR} \end{aligned} \tag{4}$$

It should be noted that the ISI is independent of the transmitting power. When adopting the modulation of BPSK (Binary Phase-Shift Keying) or QPSK, the binary sequence $\{s_n\}$ is independent and identically distributed (iid), and its average value becomes zero ($E\{s_n\} = 0$). Finally, the calculation of ISI can be simplified as

$$\mathrm{ISI} = \left(\sum\nolimits_n |K_{m-n}|^2 - \max_n |K_{m-n}|^2\right) / \max_n |K_{m-n}|^2 \tag{5}$$

As formulated in Eqs. (3) and (5), the ISI is primarily determined by K_{m-n} as well as $H(\omega + \omega_c)$. Since a wireless channel is characterized by the transfer function $H(\omega + \omega_c)$, its acquisition becomes a critical issue to evaluate our compact-range wireless access system.

B. PROPERTY OF A FINITE IMPULSE RESPONSE SYSTEM

For simplicity, a finite impulse response (FIR) system is investigated first. The ISI, as well as the delay spread due to the large aperture size of a Tx antenna, is of great interest. As illustrated in Fig. 6, the 60-GHz-band slot array antenna with $N \times N$ elements is adopted in Tx. The element spacing along both x- and y-direction is 4.2 mm in common. Hence, the aperture size can be simply calculated

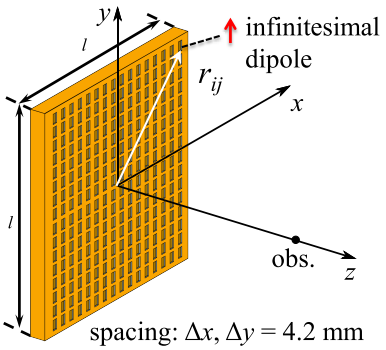

FIGURE 6. *N* × *N*-element slot array antenna with uniform distribution.

as $A = l^2 = (4.2 \times N)^2\,\mathrm{mm}^2$. An ideal corporate-fed array is assumed here. That is, there is neither frequency dependence nor delay spread inside the perfectly-matched feeding circuit. In addition, the slots are approximated by infinitesimal dipoles during the ISI analysis. Meanwhile, all dipoles are uniformly excited within the frequency band. As illustrated in Fig. 6, r_{jk} denotes the distance from the origin of coordinates to the position of the #jk dipole. When an Rx moves along the z-axis, the impulse response i.e., the transfer function, is analytically obtained as follows.

$$H(\omega + \omega_c) = \sum\nolimits_j \sum\nolimits_k E_{jk}(\omega + \omega_c) e^{-i(\omega+\omega_c)\Delta_{jk}} \tag{6}$$

$$\Delta_{jk} = \left(\sqrt{z^2 + r_{jk}^2} - \sqrt{z^2 + r_{11}^2}\right)/c \tag{7}$$

Here, E_{jk} represents the electric field, including both the near-field and far-field components, radiated from the #jk dipole. Δ_{jk} denotes the relative delay of the #jk dipole compared with the #11 one. The absolute delay time $\sqrt{z^2 + r_{11}^2}/c$, which corresponds to the transmission time from the #11 dipole to the observer, can be eliminated due to the synchronous detection widely implemented in the wireless communication systems.

The 16 × 16, 32 × 32, and 64 × 64-element arrays are assumed as the Tx antennas. At the center frequency of 60.48 GHz, their dimensions are l = 13.4 λ, 26.9 λ, and 53.8 λ, respectively. The 10-dBm input power in Tx and the 6-dBi antenna gain in Rx are chosen to coincide with the corresponding parameters adopted in our GATE demonstration [5]. At a single frequency of 60.48 GHz, we calculate the received power first as a function of the propagation distance z. It can be treated as the transfer function of the wireless channel with interest. As summarized in Fig. 7 (*a*), the dot denotes the far-field's start point, and the received power oscillates within the near-field region. It is worthwhile to note that the last minima, which are closest to those dots for the 16 × 16, 32 × 32, and 64 × 64-element arrays, lie at the positions of around z = 0.1 m, 0.5 m, and 2 m, respectively. When an Rx approaches those positions, the received power may decrease drastically. Especially if it cannot be recovered satisfactorily by an automatic gain controller (AGC), which has been included in our prototype GATE, the overall system

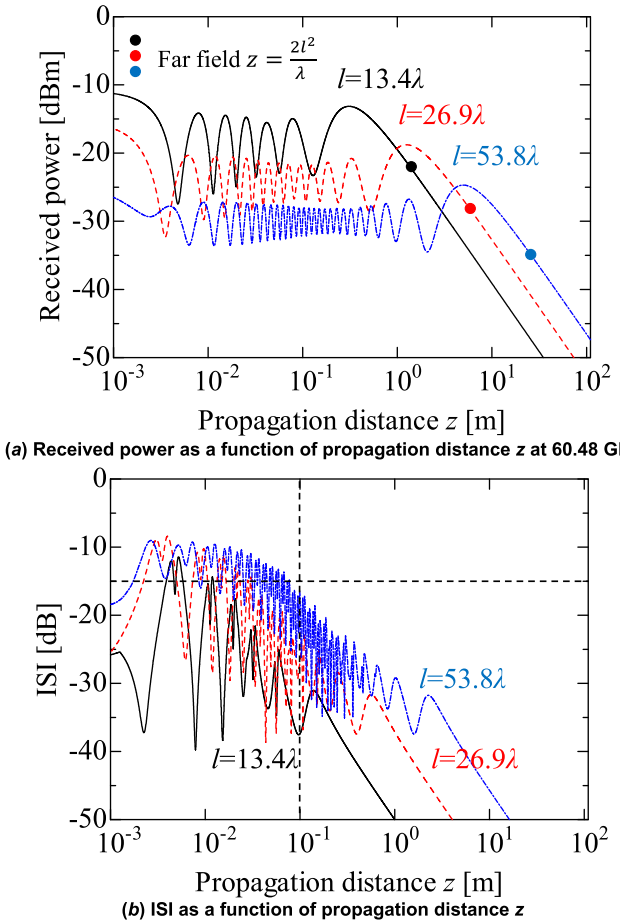

FIGURE 7. Calculated received power and ISI as a function of propagation distance z for the 16 × 16-, 32 × 32- and 64 × 64-element arrays.

SINR and BER would degrade significantly as well. Similar phenomena have been observed in Fig. 2 at positions close to the abovementioned ones. Novel array aperture distributions have been studied and proposed [27] to reduce the ripples and degradations in system performance observed in Figs. 2 and 7.

Then, by extending the transfer functions through the full spectrum of Channel 2, the ISIs' dependence on the propagation distance z are analyzed for three considered arrays. As shown in Fig. 7 (b), the ISI also oscillates in the near-field region of a Tx antenna, and it decreases monastically in the far-field region. For all Tx antennas, enlarging z longer than 10 cm leads to sufficient ISI suppression below −15 dB. In other words, this ISI due to the large aperture size of a Tx antenna may be dominant for a short distance less than 10 cm. When we compare the results shown in Fig. 2 (a) and 7 (b), to some extent, it explains the reason why the SNR degrades significantly for an extremely short distance.

Moreover, the ISI may be significantly degraded due to the multiple reflections between the Tx and Rx antennas. This effect has not been taken into account yet. In addition, an actual array antenna in Tx, which has imperfect matching and the frequency dispersion within the feeding circuit, may

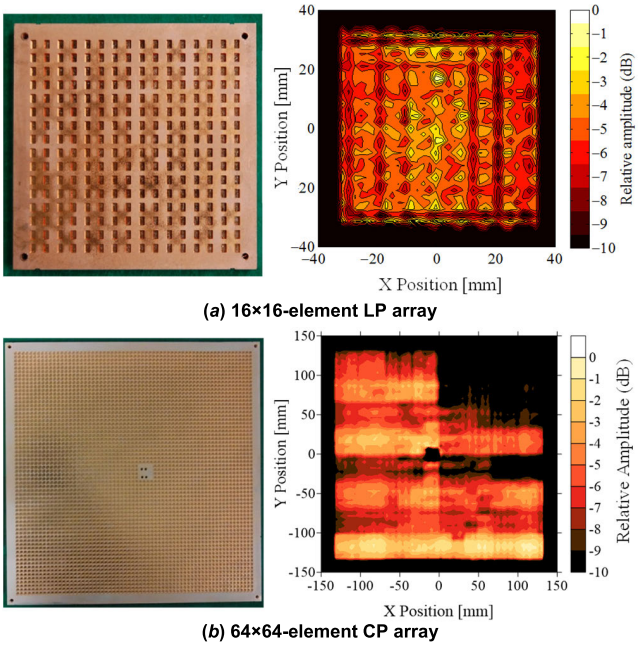

FIGURE 8. Photographs and aperture distributions of the 16 × 16- and 64 × 64-element arrays under investigation.

further degrade the system performance in terms of both SIR and BER. Those two contributions can be modeled by an infinite impulse response system rather than an FIR system investigated above.

C. PROPERTY OF AN INFINITE IMPULSE RESPONSE SYSTEM

Now, an infinite impulse response (IIR) system is studied. The degradation of ISI as well as the system performance due to the multiple reflections within or/and between Tx and Rx antennas, are to be investigated. In contrast with the previous FIR system, an experimental approach is adopted in dealing with this IIR system.

Two types of 60-GHz-band corporate-fed waveguide slot arrays are prepared to evaluate $H(\omega + \omega_c)$. One is the LP 16 × 16-element array [28]; the other one is the CP 64 × 64-element array [5], [20]. Both of them are fabricated by a process called "diffusion bonding of thin copper plates" [29], [30]. Fig. 8 shows the photographs of the considered antennas. Their performances are profoundly different: the LP 16 × 16-element array has wideband operations in both antenna gain and impedance matching; the narrowband CP 64 × 64-element array, which has been used in the previous GATE demonstration, has poor performances of both impedance matching and aperture uniformity as detailed in [5]. Their antenna sizes are 75 × 75.5 and 277 × 278 mm^2, respectively. Using a near-field measurement system, the aperture distributions for both antennas are evaluated at 60.5 GHz and included in Fig. 8, where a critical degradation in uniformity is obviously observed in the 64 × 64-element array.

1) ISI OF A 16 × 16-ELEMENT ARRAY IN TX

The ISI of an IIR system adopting the 16 × 16-element array as a Tx antenna is evaluated first. An open-ended waveguide probe in the V-band is used as the Rx antenna. This time, the transfer function is directly measured by connecting both Tx and Rx antennas to a VNA. Here, the Tx-Rx distance is selected at 70 cm, where the ISI due to the antenna aperture size is negligible according to the analysis result shown in Fig. 7 (*b*). To investigate the phenomenon of multiple reflections between Tx and Rx antennas, we also focus on the probe antenna with different installation conditions, as shown in Fig. 9. Covering a waveguide flange with a reflector or an absorber is equivalent to changing its RCS and the loop gain of this IIR system. As summarized in Fig. 10, the frequency characteristics of the transmission coefficients S_{21} between Tx and Rx antennas are measured for those three conditions. The transmission phase $\angle S_{21}$ has been modified by subtracting the absolute phase delay $\omega\tau$. Here, τ is the transmission time to synchronize the Tx and Rx antennas equivalently. When covering the waveguide flange with a reflector, we obviously observe the appearance of small ripples in the measured S_{21} as shown in Fig. 10. That is, the phenomenon of multiple reflections becomes prominent. The periodicity p_r of those ripples measured in frequency domain tightly relates to the round-trip distance l_r between Tx and Rx antennas, since the product of those two values equals the velocity of light c. Here, the periodicity read from Fig. 10 is $p_r = 0.214$ ($\approx$ 1.5/7) GHz, and then the corresponding Tx-Rx distance $l_r/2$ can also be estimated at just 70.0 cm for verification.

FIGURE 9. Open-ended waveguide probe antenna with a flange covered by an absorber and a reflector.

The measured S_{21} behaves as the transfer function $H(\omega + \omega_c)$ of the wireless channel including the antennas under investigation. By substituting it into (3), we calculate the interference sequence K_{m-n} first. As summarized in Fig. 11 (*a*), the phenomenon of multiple reflections is clearly observed for $k = m - n = 8$ when covering the waveguide flange with a reflector. There is no wonder that K_0 holds the maximum value due to the modification of $\angle S_{21}$ mentioned above. Then, by substituting those values of $|K_{m-n}|$ into (5), we evaluate ISIs as shown in Fig. 11 (*b*), where the horizontal axis $|k|$ denotes the number of symbols in calculating ISIs for sufficient convergence. A large number of $|k|$ is required, especially when a considerable delay occurs within the wireless channel. Its value is fixed at 20 throughout this paper. It is evident in Fig. 11 that the ISI performance is improved by covering the waveguide flange with an absorber,

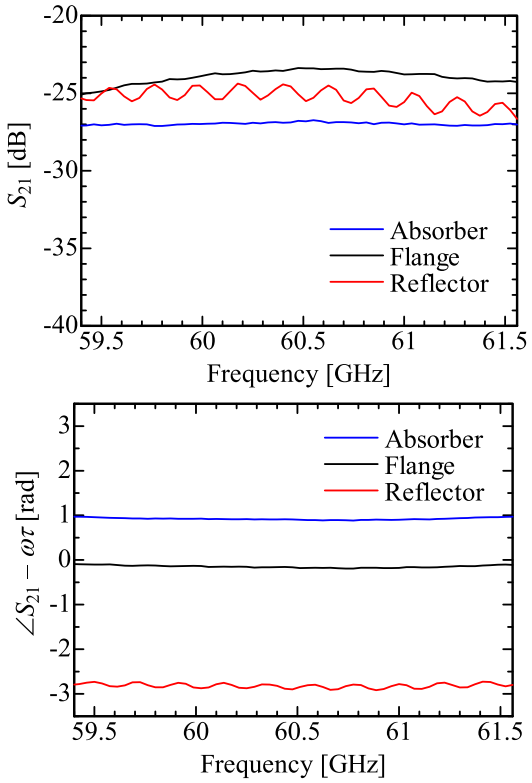

FIGURE 10. Measured S_{21} in frequency domain between a 16 × 16-element array and an open-ended waveguide probe antenna with various installation conditions. (Tx-Rx distance is 70 cm).

and on the contrary is significantly degraded by replacing the absorber with a reflector. Nonetheless, for all three conditions, error-free communication can be maintained in our GATE system, since the ISIs are sufficiently suppressed below −20 dB. It is concluded that the multiple reflections between Tx and Rx antennas do not contribute to critical ISIs when simultaneously adopting the 16 × 16-element array in Tx and separating the Tx and Rx antennas at a distance of 70 cm. Moreover, by using the VNA we also measure S_{21} in the time domain, as shown in Fig. 12 (*a*). Good similarity has been observed in Fig. 11 (*a*) since the horizontal axis $k(= m - n)$ can also be treated as the discrete time by multiplying k with the symbol length T.

2) ISI OF A 64 × 64-ELEMENT ARRAY IN TX

Lastly, the ISI of an IIR system is analyzed again by replacing the 16 × 16-element array with the 64 × 64-element one in Tx. The open-ended waveguide probe with the absorber-covered flange is used as the Rx antenna as before. This time, the Tx-Rx distance is fixed at 50 and 100 cm for comparison. As summarized in Fig. 13, the frequency characteristics of S_{21} are measured again for both distances. Similar to Fig. 10 (*b*), the absolute phase delay $\omega\tau$ has been subtracted from the raw data of $\angle S_{21}$. Especially for the distance of 50 cm, critical frequency dependence, as well as large ripples with distinct periodicity, are observed in

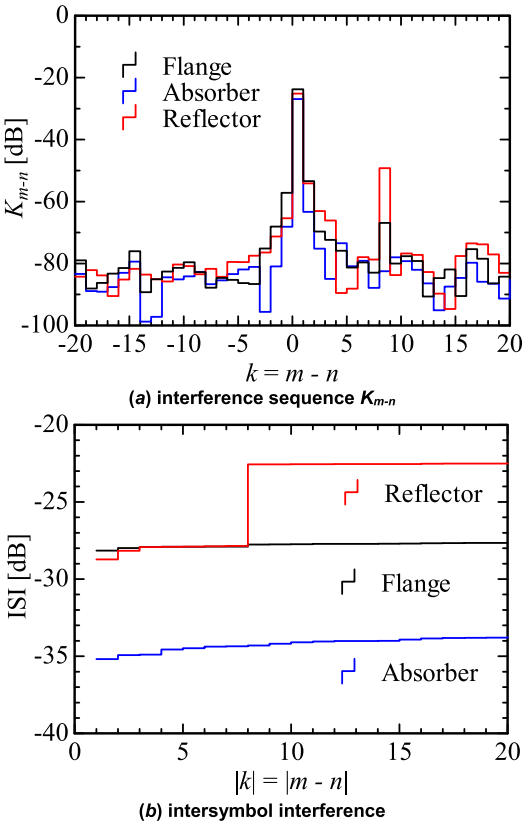

FIGURE 11. Evaluated K_{m-n} and ISI of the wireless channel using a 16 × 16-element array and an open-ended waveguide probe antenna with various installation conditions. (Tx-Rx distance is 70 cm).

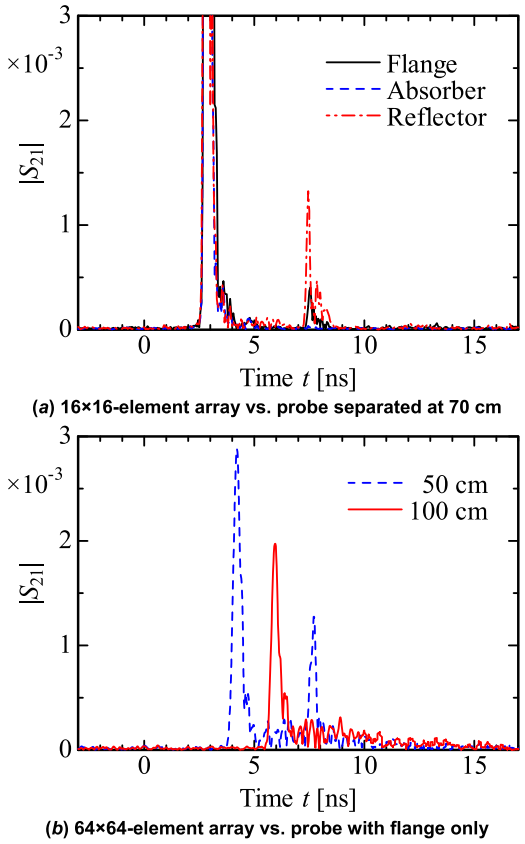

FIGURE 12. Measured S_{21} in time domain between the fabricated array antennas and an open-ended waveguide probe antenna separated at various distances.

both amplitude and phase of S_{21}. The periodicity of about 300 MHz observed in the frequency domain corresponds to the round-trip distance of 100 cm, which is exactly equal to twice the Tx-Rx distance of 50 cm. It means the phenomenon of large ripples in S_{21} mainly results from the multiple reflections between Tx-Rx antennas.

By following the similar procedures illustrated previously, again we evaluate K_{m-n} and ISI in order and summarize them in Fig. 14. The ISI (=1/SIR) degrades at as high as −6.3 dB for a Tx-Rx distance of 50 cm, and it recovers to −11.9 dB when enlarging the distance to 100 cm. By the way, an error-free communication cannot be maintained in our present GATE system [5] for the SINR lower than 11 dB.

For more detailed investigations, we remeasure the system SINR and BER as a function of the Tx-Rx distance. For each specified distance, the transfer function $H(\omega+\omega_c)$ is acquired by connecting both Tx and Rx antennas to a VNA. The evaluated SIR = 1/SIR and the measured SINR are compared in Fig. 15, where a similar tendency has been observed. Generally, the SIR is better than the SINR, where all the noise figures are included. It is uncommon that the SIR is worse than the SINR for the Tx-Rx distance of 50 cm, where the multiple reflections between Tx and Rx antennas become prominent. Nonetheless, it is still reasonable since the overall system SINR can be improved in part by an equalizer installed in the prototype GATE [17]. To some extent, those calculated SIRs qualitatively interpret the reason why the BER degrades for the propagation distance $z < 1$ m, as illustrated in Fig. 2.

On the other hand, according to the calculated ISIs summarized in Figs. 7 (*b*) and 11 (*b*), neither the large antenna size nor the multiple reflections between Tx and Rx antennas contributes to the ISI as high as −11.9 dB for a Tx-Rx distance of 100 cm. It is suspected that the multiple reflections within the feeding circuit of the Tx antenna itself, which were neglected in our previous analysis, becomes the primary contribution.

When separating the Tx and Rx antennas at 50 and 100 cm, S_{21} are also measured in the time domain. As summarized in Fig. 12 (*b*), small ripples closely follow the principle transmitted-wave for either antenna distance of 50 cm or 100 cm. Those two curves behave in very similar manners and tightly relate to the Tx antenna's performance. According to our investigation, those small ripples, caused by the multiple reflections within the antenna feeding circuit, may lead to the degradation in both overall antenna reflections and system ISIs. In that sense, it becomes essential to sufficiently suppress multiple reflections within or/and between the Tx and Rx antennas adopted in a compact-range wireless access system.

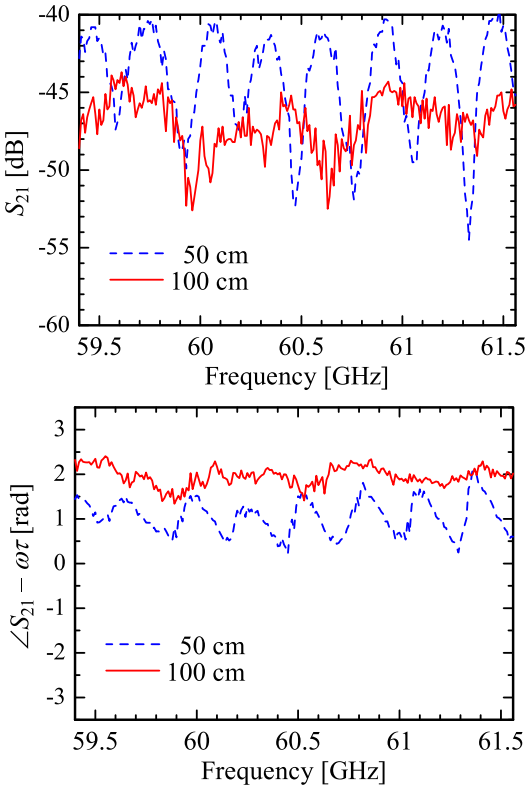

FIGURE 13. Measured S_{21} in frequency domain between a 64 × 64-element array and an open-ended waveguide probe antenna separated at various distances.

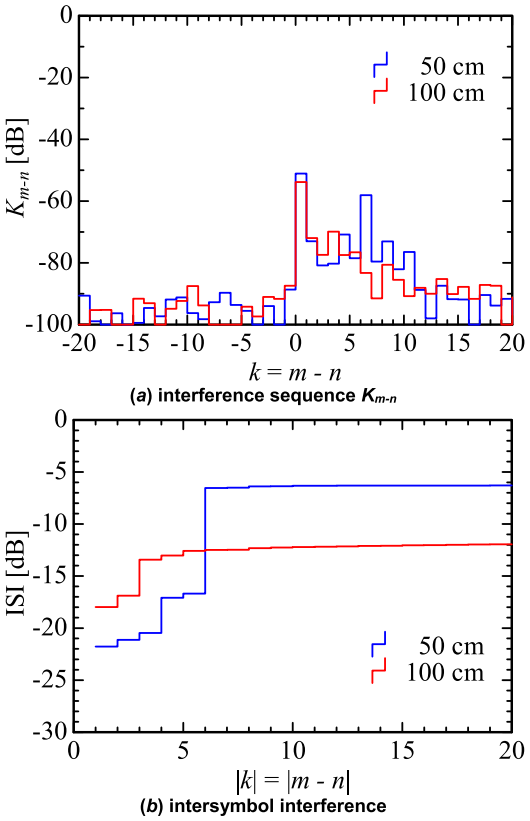

FIGURE 14. Evaluated interference sequence and ISI of the wireless channel using a 64 × 64-element array for various distances.

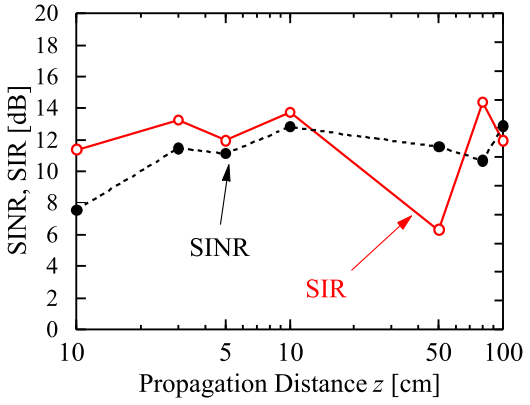

FIGURE 15. Comparison between measured SINR and evaluated SIR for various antenna distances.

Three contributions to ISIs have been investigated in detail. It is worth noting that the ISI, due to the multiple reflections within a Tx antenna, is independent of the propagation distance but determines the noise floor level in our GATE system. On the other hand, the ISIs, due to the large antenna aperture size and the multiple reflections between the Tx and Rx antennas, have a large dependence on the propagation distance. Especially for a short distance, their contributions to ISIs become dominant. This unique phenomenon is distinct from what occurs in a multipath-rich environment typical for a conventional mobile communication system. Those three contributions to ISIs lead to significant degradations in both SINR and BER for a short distance, while the system performance can recover to some extent for a long distance.

As a short conclusion, when adopting a 64 × 64-element array in Tx, the system performance in terms of SINR and BER tightly relates to the abovementioned three factors of ISIs with various distance dependence. According to our detailed investigation, the ISI due to the large aperture size becomes dominant for a Tx-Rx distance shorter than 10 cm and can be reduced below −15 dB for a longer distance. Meanwhile, at a Tx-Rx distance around 50 cm, the multiple reflections between Tx and Rx antennas significantly degrade not only the ISI but also the overall system SINR and BER. On the other hand, rather than ISI, the Rx-RF signal level decreases drastically around 2 m due to the destructive interference resulting from the large aperture size as predicted in Fig. 7 (*a*), and its insufficient recover also leads to the degradation in both SINR and BER.

Generally, even for the near-field applications, the corporate-fed array still has considerable advantages over the series-fed one in terms of bandwidth, delay, and ISI. Nonetheless, the series-fed array is still applicable for a limited aperture size and remains as attractive due to its simple structure as well as low cost.

V. CONCLUSION

The intersymbol interference occurring in the 60-GHz-band compact-range wireless system adopting a large array antenna has been analyzed. An equivalent baseband communication system is newly proposed to evaluate the wireless channel, including Tx and Rx antennas. As an FIR system, the ISI, due to the large aperture size of a Tx antenna, has been investigated first. An IIR system considering the multiple reflections within or/and between Tx and Rx antennas has been investigated as well. The calculated SIR (=1/ISI) behave in a similar tendency with the measured SINR. Those results qualitatively interpret the reason why the BER degrades for the propagation distance $z < 1$ m. Furthermore, as future work, the proposed ISI analysis can help us draw up new guidelines on designing large array antennas. It also has extensive applications to evaluating other wideband systems.

REFERENCES

[1] *Technical Feasibility of IMT in Bands Above 6 GHz*, document ITU-R M.2376, Jul. 2015.
[2] *Framework and Overall Objectives of the Future Development of IMT for 2020 and Beyond*, document ITU-R M.2083, Sep. 2015.
[3] S. Rangan, T. S. Rappaport, and E. Erkip, "Millimeter-wave cellular wireless networks: Potentials and challenges," *Proc. IEEE*, vol. 102, no. 3, pp. 366–385, Mar. 2014.
[4] K. Sakaguchi, G. K. Tran, H. Shimodaira, S. nanba, T. Sakurai, K. Takinami, I. Siaud, E. C. Strinati, A. Capone, I. Karls, R. Arefi, and T. Haustein, "Millimeter-wave evolution for 5G cellular networks," *IEICE Trans. Commun.*, vol. 98, no. 3, pp. 388–402, Mar. 2015.
[5] M. Zhang, K. Toyosaki, J. Hirokawa, M. Ando, T. Taniguchi, and M. Noda, "A 60-GHz band compact-range gigabit wireless access system using large array antennas," *IEEE Trans. Antennas Propag.*, vol. 63, no. 8, pp. 3432–3440, Aug. 2015.
[6] S. Haykin, *Communication Systems*, vol. 2, 4th ed. New York, NY, USA: Wiley, 2001, pp. 259–267.
[7] Z. N. Low, J. H. Cheong, and C. L. Law, "Low-cost PCB antenna for UWB applications," *IEEE Antennas Wireless Propag. Lett.*, vol. 4, pp. 237–239, 2005.
[8] B. S. Yildirim, B. A. Cetiner, G. Roqueta, and L. Jofre, "Integrated Bluetooth and UWB antenna," *IEEE Antennas Wireless Propag. Lett.*, vol. 8, pp. 149–152, 2009.
[9] G. Adamiuk, T. Zwick, and W. Wiesbeck, "UWB antennas for communication systems," *Proc. IEEE*, vol. 100, no. 7, pp. 2308–2321, Jul. 2012.
[10] M. B. Gueye, H. H. Ouslimani, S. N. Burokur, A. Priou, Y. Letestu, and A. Le Bayon, "Antenna array for point-to-point communication in E-band frequency range," in *Proc. IEEE Int. Symp. Antennas Propag. (APSURSI)*, Jul. 2011, pp. 2077–2079.
[11] M. Zhang, J. Hirokawa, and M. Ando, "An E-band partially corporate feed uniform slot array with laminated quasi double-layer waveguide and virtual PMC terminations," *IEEE Trans. Antennas Propag.*, vol. 59, no. 5, pp. 1521–1527, May 2011.
[12] N. Ghassemi and K. Wu, "High-efficient patch antenna array for E-band gigabyte point-to-point wireless services," *IEEE Antennas Wireless Propag. Lett.*, vol. 11, pp. 1261–1264, 2012.
[13] I. Papageorgiou, A. Derneryd, L. Manholm, and J. Yang, "An E-band cylindrical reflector antenna for wireless communication systems," in *Proc. 7th Eur. Conf. Antennas Propag.*, 2013, pp. 524–528.
[14] T. Tomura, J. Hirokawa, T. Hirano, and M. Ando, "A 45° linearly polarized hollow-waveguide 16×16-slot array antenna covering 71-86 GHz band," *IEEE Trans. Antennas Propag.*, vol. 62, no. 10, pp. 5061–5067, Oct. 2014.
[15] A. Hirata, H. Takahashi, J. Takeuchi, N. Kukutsu, D. Kim, and J. Hirokawa, "120-GHz-band antenna technologies for over-10-Gbps wireless data transmission," in *Proc. 6th Eur. Conf. Antennas Propag. (EUCAP)*, Mar. 2012, pp. 2564–2568.
[16] D. Kim, J. Hirokawa, M. Ando, J. Takeuchi, and A. Hirata, "64×64-element and 32×32-element slot array antennas using double-layer hollow-waveguide corporate-feed in the 120 GHz band," *IEEE Trans. Antennas Propag.*, vol. 62, no. 3, pp. 1507–1512, Mar. 2014.
[17] Y. Asakura, K. Kondou, M. Shinagawa, S. Tamonoki, and M. Noda, "Prototype of 3-Gb/s 60-GHz millimeter-wave-based wireless file-transfer system," in *Proc. URSI Commission B Int. Symp. Electromagn. Theory (EMTS)*, Hiroshima, Japan, May 2013, pp. 207–210.
[18] K. Okada, K. Kondou, M. Miyahara, M. Shinagawa, H. Asada, R. Minami, T. Yamaguchi, A. Musa, Y. Tsukui, Y. Asakura, and S. Tamonoki, "Full four-channel 6.3-Gb/s 60-GHz CMOS transceiver with low-power analog and digital baseband circuitry," *IEEE J. Solid-State Circuits*, vol. 48, no. 1, pp. 46–65, Jan. 2013.
[19] H. Yamagishi and M. Noda, "High throughput hardware architecture for (1440,1344) low-density parity-check code utilizing quasi-cyclic structure," in *Proc. 5th Int. Symp. Turbo Codes Rel. Topics*, Sep. 2008, pp. 78–83.
[20] M. Zhang, J. Hirokawa, and M. Ando, "Waveguide slot antennas with different aperture sizes developed for the MMW short range wireless access gate system," in *Proc. Int. Symp. Antennas Propag. (ISAP)*. Nagoya, Japan: Nagoya Congress Center, Oct./Nov. 2012, pp. 259–262.
[21] A. Goldsmith, *Wireless Communication*. New York, NY, USA: Cambridge Univ. Press, 2005, pp. 184–187.
[22] R. C. Hansen, "Relationships between antennas as scatterers and as radiators," *Proc. IEEE*, vol. 77, no. 5, pp. 659–662, May 1989.
[23] E. F. Knott, J. F. Shaeffer, M. T. Tuley, *Radar Cross Section*, 2nd ed. Raleigh, NC, USA: SciTech, 2004, pp. 259–261.
[24] T. P. Do, K. Araki, J. Hirokawa, and M. Ando, "Signal flow graph model for distance-dependent transfer function between two antennas in short-range communication," in *Proc. Int. Symp. Antennas Propag. (ISAP)*, Ginowan, Japan, vol. 63, Oct. 2016, pp. 836–837.
[25] M. Ali and M. Ando, "Fast estimation of field in the shadow zone for finite cylindrical structures by modified edge representation (MER) in compact range communication," *IEICE Trans. Commun.*, vol. E99.B, no. 7, pp. 1541–1549, Jul. 2016.
[26] M. Zhang, K. Araki, J. Hirokawa, and M. Ando, "Intersymbol interference analysis of a 60 GHz-band compact range wireless access system," in *Proc. 9th Eur. Conf. Antennas Propag. (EuCAP)*, Lisbon, Portugal, Apr. 2015, pp. 1–4.
[27] D. Mohri, M. Ando, and J. Hirokawa, "Non-linear optimization of the excitation coefficients of an array antenna of large-number elements to reduce the amplitude ripples in the mm-wave hotspot area illumination," in *Proc. Int. Symp. Antennas Propag. (ISAP)*, Ginowan, Japan, 2016, pp. 834–835.
[28] T. Tomura, J. Hirokawa, T. Hirano, and M. Ando, "A wideband 16 × 16-element corporate-feed hollow-waveguide slot array antenna in the 60-GHz band," *IEICE Trans. Commun.*, vol. E97.B, no. 4, pp. 798–806, 2014.
[29] R. W. Haas, D. Brest, H. Mueggenburg, L. Lang, and D. Heimlich, "Fabrication and performance of MMW and SMMW platelet horn arrays," *Int. J. Infr. Millim. Waves*, vol. 14, no. 11, pp. 2289–2294, Nov. 1993.
[30] M. Zhang, J. Hirokawa, and M. Ando, "Design of a partially-corporate feed double-layer slotted waveguide array antenna in 39 GHz band and fabrication by diffusion bonding of laminated thin metal plates," *IEICE Trans. Commun.*, vol. E93-B, no. 10, pp. 2538–2544, 2010.

MIAO ZHANG (Senior Member, IEEE) received the B.S., M.S., and D.E. degrees in electrical and electronic engineering from the Tokyo Institute of Technology, Tokyo, Japan, in 2003, 2005, and 2008, respectively.

From 2005 to 2008, he was a Research Fellow with the Japan Society for the Promotion of Science, Tokyo. Since 2008, he has been a Researcher with the Tokyo Institute of Technology, and he became an Assistant Professor, in 2013. He is currently an Associate Professor with Xiamen University, China. His research interests include waveguide slot arrays, millimeter-wave antennas, and array antennas for 5G and car-radar applications. He is also a Senior Member of CIE and IEICE. He was a recipient of the Best Letter Award from the IEICE Communication Society, in 2009, the Young Engineer Award from the IEICE Technical Committee on Antennas and Propagation, in 2010, the IEEE AP-S Japan Chapter Young Engineer Award, in 2011, and the Best Paper Award at the 9th European Conference on Antennas and Propagations, in 2015.

MASAHIRO WAKASA received the B.S. and M.S. degrees in electrical and electronic engineering from the Tokyo Institute of Technology (Tokyo Tech), Tokyo, Japan, in 2015 and 2018, respectively.

KOJI TOYOSAKI received the B.S. and M.S. degrees in electrical and electronic engineering from the Tokyo Institute of Technology (Tokyo Tech), Tokyo, Japan, in 2014 and 2016, respectively.

KIYOMICHI ARAKI (Life Member, IEEE) received the Ph.D. degree in physical electronics from the Tokyo Institute of Technology, Tokyo, Japan, in 1978. From 1973 to 1975 and from 1978 to 1985, he was a Research Associate with the Tokyo Institute of Technology. From 1985 to 1995, he was an Associate Professor with Saitama University, Saitama, Japan. From 1979 to 1980 and from 1993 to 1994, he was a Visiting Research Scholar with The University of Texas at Austin, Austin, TX, USA, and the University of Illinois at Urbana-Champaign, Champaign, IL, USA. From 1995 to 2014, he was a Professor with the Tokyo Institute of Technology. He has numerous journals and peer-reviewed publications in RF ferrite devices, RF circuit theory, electromagnetic field analysis, software-defined radio, array signal processing, UWB technologies, wireless channel modeling, MIMO communication theory, digital RF circuit design, information security, and coding theory. He has been a Fellow of IEICE, since 2004. He is also the President-Elect of the Electronics Society of IEICE of Japan and a member of IEE and the Information Processing Society of Japan. He was awarded the Best Paper Award, in 2007. He has served as a Steering Committee Chair for APMC 2010. He is also the Chair of the MTT-S Japan Chapter. He was the Director/Finance of IEICE, in 2013.

JIRO HIROKAWA (Fellow, IEEE) received the B.S., M.S., and D.E. degrees in electrical and electronic engineering from the Tokyo Institute of Technology (Tokyo Tech), Tokyo, Japan, in 1988, 1990, and 1994, respectively. He was a Research Associate, from 1990 to 1996, and an Associate Professor, from 1996 to 2015, with Tokyo Tech. He was with the Antenna Group, Chalmers University of Technology, Gothenburg, Sweden, as a Postdoctoral Fellow, from 1994 to 1995. He is currently a Professor with Tokyo Tech. His research interests include slotted waveguide array antennas and millimeter-wave antennas. He is also a Fellow of IEICE. He received the IEEE AP-S Tokyo Chapter Young Engineer Award, in 1991, the Young Engineer Award from IEICE, in 1996, the Tokyo Tech Award for Challenging Research, in 2003, the Young Scientists' Prize from the Minister of Education, Culture, Sports, Science and Technology, Japan, in 2005, the Best Paper Award, in 2007, the Best Letter Award from the IEICE Communications Society, in 2009, and the IEICE Best Paper Award, in 2016 and 2018.

MAKOTO ANDO (Life Fellow, IEEE) was born in Hokkaido, Japan, in February 1952. He received the B.S., M.S., and D.E. degrees in electrical engineering from the Tokyo Institute of Technology, Tokyo, Japan, in 1974, 1976, and 1979, respectively.

From 1979 to 1983, he worked with the Yokosuka Electrical Communication Laboratory, NTT, and was involved in development of antennas for satellite communication. He was a Research Associate with the Tokyo Institute of Technology, from 1983 to 1985, where he is currently a Professor. His current interests include high-frequency diffraction theory, such as physical optics and geometrical theory of diffraction, the design of reflector antennas and waveguide planar arrays for DBS and VSAT, and the design of high-gain millimeter-wave antennas. He was a recipient of the Young Engineers Award of IEICE, Japan, in 1981, and the Achievement Award and the Paper Award from IEICE, in 1993. He was also a recipient of the 5th Telecom Systems Award, in 1990, the 8th Inoue Prize for Science, in 1992, the Meritorious Award of the Minister of Internal Affairs and Communications and the Chairman of the Broad of ARIB, in 2004, the Award in Information Promotion Month 2006 of the Minister of Internal Affairs and Communications, and the IEICE Distinguished Achievement and Contributions Award, in 2014. He has served as the Chair of Commission B for URSI, from 2002 to 2005, and a member of Administrative Committee of the IEEE Antennas and Propagation Society, from 2004 to 2006. He was the Chair of the Technical committee of Electromagnetic theory, from 2004 to 2005, and Antennas and Propagation, from 2005 to 2007, in IEICE. He was the General Chair of the 2004 URSI EMT Symposium in Pisa and the ISAP 2007 in Niigata. He was the 2007 President of Electronics Society IEICE and the 2009 President of the IEEE Antennas and Propagation Society. He was the 2018 President of IEICE. He is also the President of URSI. He has also served as the Program Officer for engineering science group in the Research Center for Science Systems, JSPS, from 2007 to 2009. He has served as the Guest Editor-in-Chief for more than six special issues in IEICE, *Radio Science*, and the IEEE TRANSACTIONS ON ANTENNAS AND PROPAGATION (AP).